



LAWRENCE
LIVERMORE
NATIONAL
LABORATORY

Simulated and experimental compression of a compact toroid

J. N. Johnson, D. Q. Hwang, R. D. Horton, R. W.
Evans, J. M. Owen

May 8, 2009

Applied Physics Letters

Disclaimer

This document was prepared as an account of work sponsored by an agency of the United States government. Neither the United States government nor Lawrence Livermore National Security, LLC, nor any of their employees makes any warranty, expressed or implied, or assumes any legal liability or responsibility for the accuracy, completeness, or usefulness of any information, apparatus, product, or process disclosed, or represents that its use would not infringe privately owned rights. Reference herein to any specific commercial product, process, or service by trade name, trademark, manufacturer, or otherwise does not necessarily constitute or imply its endorsement, recommendation, or favoring by the United States government or Lawrence Livermore National Security, LLC. The views and opinions of authors expressed herein do not necessarily state or reflect those of the United States government or Lawrence Livermore National Security, LLC, and shall not be used for advertising or product endorsement purposes.

Simulated and experimental compression of a compact toroid

J. N. Johnson,* D. Q. Hwang, R. D. Horton, R. W. Evans, and J. M. Owen

University of California, Davis

(Dated: May 6, 2009)

We present simulation results and experimental data for the compression of a compact toroid by a conducting nozzle without a center electrode. In both simulation and experiment, the flow of the plasma is greatly obstructed by even modest magnetic fields. A simple mechanism for this obstruction is suggested by our simulations. In particular, the configuration of the plasmoid's magnetic field plays a significant role in the success of the experiment. We analyze two types of plasma configurations under compression and demonstrate that the results from the simulations matches those from the experiments, and that the mechanism predicts the different behaviors observed in the two cases.

Plasmoids¹, or self-contained magnetized plasmas, hold much promise as a mechanism for energy transport². In particular, many groups have studied the acceleration of spheromak-like configurations such as compact toroids (CTs)³⁻⁵. In the U.C. Davis Compact Toroid Injection eXperiment (CTIX)⁶, a plasma is created from a neutral gas, seeded with a poloidal magnetic field from a solenoid, and then allowed to equilibrate to a quasi-force-free configuration. This plasma is then accelerated between two concentric electrodes with magnetic pressure maintained by currents discharged from a capacitor bank. The plasma can achieve velocities near 200 km/s, and the peak number density is typically around $10^{15}/\text{cc}$. The maximum velocity of the plasma is limited by the circuit and possibly by the blowby instability³, so raising the density of the plasma seems a better way to deliver more energy.

One way to increase the density is to compress the plasma after it has been accelerated. To this end, the CTIX group has constructed a conical compression nozzle with an area ratio of 10:1. This nozzle is placed after the terminus of the center electrode, so the compression occurs while the plasma is drifting freely. In this letter we present the results of our simulations of the compression and the corresponding experimental observations.

We simulate the plasma with Spasmos, a resistive magnetohydrodynamics (MHD) code that uses Smoothed Particle Hydrodynamics (SPH). The details of the algorithm will appear in J.J.'s forthcoming PhD Thesis⁷ with more information about this experiment. In short, the code solves the Lagrangian single-fluid MHD equations

$$\frac{D\rho}{Dt} = -\rho\nabla\cdot\mathbf{v} \quad (1)$$

$$\frac{D\mathbf{v}}{Dt} = \frac{\nabla\cdot\mathbf{S}}{\rho} \quad (2)$$

$$\frac{Du}{Dt} = -\frac{P}{\rho}\nabla\cdot\mathbf{v} \quad (3)$$

$$\frac{D\mathbf{B}}{Dt} = \mathbf{B}\cdot\nabla\mathbf{v} - \mathbf{B}(\nabla\cdot\mathbf{v}) + \nabla\times\left(\frac{\eta}{\mu_0}\nabla\times\mathbf{B}\right) \quad (4)$$

We have written the momentum equation in terms of the

hydromagnetic stress tensor

$$\mathbf{S} = -(P + \frac{B^2}{2\mu_0})\mathbf{I} + \frac{\mathbf{B}\mathbf{B}}{\mu_0}.$$

The quantities are defined on discrete points, or nodes, in space. Each node i represents a Lagrangian fluid element with fixed mass m_i moving at a fluid velocity \mathbf{v}_i possessing specific thermal energy u_i , magnetic field \mathbf{B}_i , and electrical resistivity η . There is no computational grid connecting the nodes; they connect to their closest neighbors dynamically. In SPH, spatial derivatives are defined in terms of a spherically-symmetric smoothing kernel $W(\mathbf{x} - \mathbf{x}'; h)$ of finite extent h so that the spatial derivatives on a node are approximated by sums of neighbor contributions weighted by their kernel gradients. In Spasmos, the MHD equations are reduced to the nodal ordinary differential equations

$$\rho_i = \sum_j m_j W_i \quad (5)$$

$$\frac{d\mathbf{v}}{dt} = -\sum_j m_j \left(\frac{\mathbf{S}_i}{\rho_i^2} + \frac{\mathbf{S}_j}{\rho_j^2} \right) \nabla W_{ij} \quad (6)$$

$$\begin{aligned} \frac{d\mathbf{B}}{dt} = & \sum_j \mathbf{B}_i \cdot (\mathbf{v}_{ij}) \nabla W_i - \mathbf{B}_i (\mathbf{v}_{ij}) \cdot \nabla W_j \\ & + \sum_j \frac{\eta_j}{\mu_0} \frac{m_j}{\rho_j} \frac{\nabla W_{ij}}{|\mathbf{x}_i - \mathbf{x}_j|^2} (\mathbf{B}_i - \mathbf{B}_j) \end{aligned} \quad (7)$$

where the subscripts identify quantities on the nodes $\{j\}$ that neighbor a node i , $\mathbf{v}_{ij} = \mathbf{v}_i - \mathbf{v}_j$, $W_i = W(\mathbf{x}_i - \mathbf{x}_j; h_i)$, $\nabla W_i = \nabla W(\mathbf{x}_i - \mathbf{x}_j; h_i)$, and $\nabla W_{ij} = (\nabla W_i + \nabla W_j)/2$ is a gradient that is symmetric between nodes i and j . In particular, the mass density is measured by the number density of the nodes weighted by their masses. The specific thermal energy is evolved by assuming that the change in purely hydrodynamic kinetic energy is balanced by a change in the thermal energy⁸, after which Joule heating is applied.

The plasma is initialized as a toroid of axial length L and inner/outer radii r_1 and r_2 with a uniform density ρ_0 , uniform energy per unit mass u_0 corresponding to temperature T_0 , and a uniform axial velocity $\mathbf{v} = (0, 0, v_0)$.



FIG. 1: Simulated plasma within the compression nozzle (quadrant). $|\mathbf{B}|$ contours demonstrate strong magnetic field (bright blob) in the center.

The magnetic field is set to a force-free state in which $(\nabla \times \mathbf{B}) \times \mathbf{B} = \mathbf{0}$ when the toroid is confined by conducting walls at $z = 0$, $z = L$, $r = r_1$ and $r = r_2$ ⁹. This is the well-known Taylor force-free state and is an idealized configuration, but is routinely used in modeling CTs in the literature. We use an ideal gas law for the plasma pressure with $\gamma = 5/3$ and a Spitzer model for the resistivity in which $\eta = 5.2 \times 10^{-15} Z \ln \Lambda T^{-3/2}$. Since the compression nozzle sits beyond the accelerator region, we do not model the center electrode in CTIX. The nozzle has maximum and minimum radii R_{max} , R_{min} , and r_2 is typically set to R_{max} . Table I shows typical values for these parameters in our simulations, which were chosen to match their experimental values.

| | | | |
|-----------|--------------|-----------|------------------------------------|
| R_{max} | 0.06391 m | R_{min} | 0.02013 m |
| r_1 | 0.0318 m | B_0 | 0.1 - 1 T |
| L | 0.05 - 0.5 m | ρ_0 | $10^{-7} - 10^{-6} \text{ kg/m}^3$ |
| T_0 | 20 - 100 eV | v_0 | 100 - 200 km/s |

TABLE I: Typical values for parameters in compression simulations.

Our simulations show that the above magnetic configuration can obstruct the flow of CTs through the nozzle, even when the field is not particularly strong. As the plasma expands, a strong magnetic field develops at the center of the vessel, pushing the plasma out against the nozzle and hindering its travel. Figure 1 shows this strongly magnetized region in the vessel, which develops shortly after the plasma leaves the center electrode.

The development of this strong magnetic field can be explained by magnetic reconnection. As the plasma leaves the center electrode, it begins expanding radially inward, carrying with it the internal magnetic field. When the plasma reaches the z axis, the magnetic field reconnects with itself. In a compact toroid, the field on the inner radius is strong and has both toroidal (B_θ) and poloidal (B_z) components. The toroidal components of the field add to zero at the center. However, the poloidal components are all aligned, so they produce a large magnetic field.

To illustrate this reconnection, we have run some planar 2D simulations of plasmoid cross sections for both a CT and a plasma jet in which $\mathbf{B} = (0, B_\theta, 0)$. Figure 2 shows the intensity of \mathbf{B} in the plasmas as the observer looks along the axis of the simulated CTIX device, both before the expansion and at later times. As we expect,

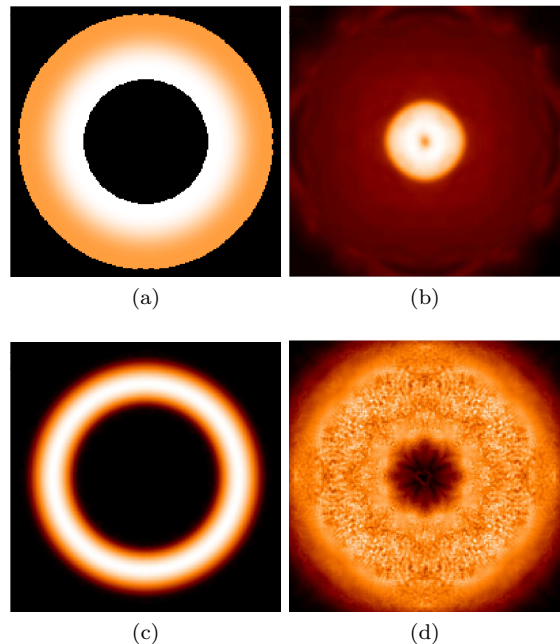


FIG. 2: 2D simulations of a cross section of an expanding plasmoid. (a) and (b) show a CT initially and after reconnection ($t = 0.1\mu\text{s}$). (c) and (d) show the initial and final configurations for a toroidal jet.

the CT field reconnects and magnetizes the center of the vessel very quickly, repelling the plasma before most of the material is allowed to inflow. The field in the jet exhibits no such reconnection, and the plasma flows inward uninhibited.

CTs generated by CTIX have magnetic fields whose strength is estimated to be between 0.5 to 1.5 T. Our simulations predict that even a 0.5 T field will not allow a CT through the nozzle at a muzzle velocity v_0 of 150 km/s. Weaker fields of 0.1-0.2 T still produce magnetic peaks in the center, but do allow a CT with $v_0 = 150$ km/s to pass. Meanwhile, plasma jets with much larger magnetic fields seem able to pass through the nozzle without much difficulty. Unfortunately, such jets are not spatially localized and make poor energy vehicles.

To validate these simulations, we ran compression experiments on both compact toroids and jets on CTIX. For shots involving CTs, we produced plasmas with various magnetic field strengths and accelerated them. Langmuir probes along the outer electrode and nozzle measured the strength of the plasma's field and verified its toroidal structure. As plasma emerged from the nozzle into a viewing chamber, its light was captured by a CCD camera. This light was used as the measure of the success or failure of the plasma to escape from the nozzle. To form toroidal plasma jets instead of CTs, we deactivated the solenoid that seeds the poloidal magnetic field in the formation section.

The data from these experiments matches our simulation results in the sense that none of the accelerated

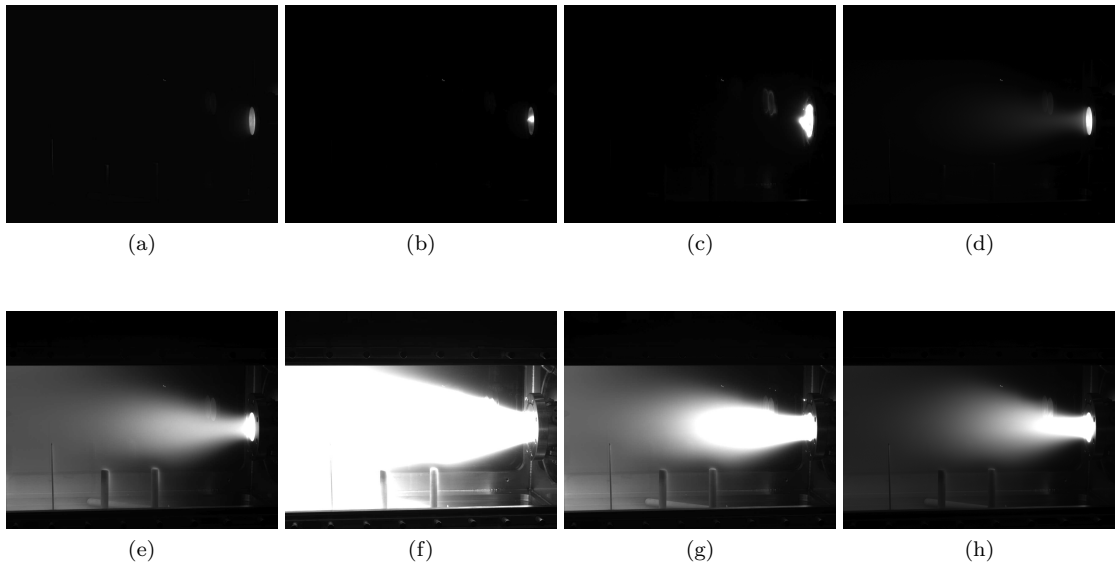


FIG. 3: Several shots of plasma emerging from the nozzle at right. (a) - (d) show CT shots, while (e) - (h) show jets with toroidal fields.

CTs were able to make it through the nozzle. Because the velocity of the CT depends on its internal magnetic field strength, it appears unlikely that CTIX can generate a weakly magnetized CT with sufficient velocity to escape the nozzle. Jets, on the other hand, emerge readily even when strong magnetic fields are present. Figure 3 shows photos taken by the CCD camera for several CTs and jets. During these shots, the sensitivity of the camera was adjusted so that ambient light would not be detected. To give the plasma ample time to make its way through the nozzle, the shutter on the camera was allowed to remain open for 1 ms, a timescale that exceeds that of a typical plasma's journey by an order of magnitude. Table II shows estimated values of the magnetic fields for the plasmas shown in Figure 3.

| Shot | a | b | c | d | e | f | g | h |
|----------------|------|------|-------|------|--------|-------|-------|------|
| B_z (T) | 0.27 | 0.13 | 0.068 | 0.24 | 0.0018 | 0.018 | 0.053 | 0.15 |
| B_θ (T) | 0.20 | 0.14 | 0.17 | 0.27 | 0.32 | 0.53 | 0.40 | 0.32 |

TABLE II: Estimated peak magnetic field measurements for shots in Figure 3. These fields are measured as the plasma enters the nozzle.

This work performed under the auspices of the U.S. Department of Energy by Lawrence Livermore National Laboratory under Contract DE-AC52-07NA27344.

* Electronic address: jnjohnso@ucdavis.edu

¹ W. H. Bostick, in *Electromagnetic Phenomena in Cosmical Physics* (1958), vol. 6.

² W. A. Newcomb, *Phys. Fluids*. B **3**, 1818 (1991).

³ K. L. Baker, D. Q. Hwang, R. W. Evans, R. D. Horton, H. S. McLean, S. Terry, S. Howard, and C. J. DiCaprio, *Journal of Fusion Energy* **42**, 94 (2002).

⁴ R. Raman, *Phys. Rev. Lett.* **73**, 3101 (1994).

We have used Spasmos, an SPH resistive MHD code, to simulate the unaccelerated compression of magnetized plasmas in the CTIX device, obtaining results consistent with those of experiment. The simulations predict a reconnection mechanism that disrupts the flow of the plasma by strongly magnetizing the center of the vessel. The reconnection is associated with poloidal magnetic field, since the axial components from the field lines are aligned. This suggests that unaccelerated compression is not a promising approach for plasmoids with appreciable poloidal magnetic fields, such as CTs and reverse field configurations.

A more attractive means of compression may be to continue the acceleration of the plasma into the nozzle. In this scenario, the inner electrode would continue into the compression section and taper as needed. The presence of a center electrode within the nozzle would disallow the reconnection that impedes the flow of the plasma, and the added kinetic energy would help against the magnetic pressure under compression. The simulation of such a process can be explored in the near future.

J.J. is supported by the Lawrence Scholar Program at Lawrence Livermore National Laboratory.

⁵ M. R. Brown and P. M. Bellan, *Nucl. Fusion* **32**, 1125 (1992).

⁶ D. Q. Hwang, R. D. Horton, S. Howard, R. W. Evans, and S. E. Brockington, *Journal of Fusion Energy* **1**, 81 (2006).

⁷ J. N. Johnson, Ph.D. thesis, Univ. of California, Davis (2009).

⁸ J. M. Owen (2007).

⁹ S. Howard, Ph.D. thesis, Univ. of California, Davis (2006).